Biochimica et Biophysica Acta 1848 (2015) 1119–1126

Contents lists available at ScienceDirect

Biochimica et Biophysica Acta

journal homepage: www.elsevier.com/locate/bbamem

Dengue virus NS4A cytoplasmic domain binding to liposomes is sensitive to membrane curvature

Yu-Fu Hung [a,b], Melanie Schwarten [a], Sven Schünke [a,1], Pallavi Thiagarajan-Rosenkranz [a,2], Silke Hoffmann [a], Ella H. Sklan [c], Dieter Willbold [a,b], Bernd W. Koenig [a,b,*]

[a] Institute of Complex Systems, Structural Biochemistry (ICS-6), Forschungszentrum Jülich, 52425 Jülich, Germany
[b] Institut für Physikalische Biologie, Heinrich-Heine-Universität Düsseldorf, Universitätsstraße 1, 40225 Düsseldorf, Germany
[c] Department Clinical Microbiology and Immunology, Sackler School of Medicine, Tel Aviv University, Tel Aviv 69978, Israel

ARTICLE INFO

Article history:
Received 26 September 2014
Received in revised form 23 December 2014
Accepted 21 January 2015
Available online 30 January 2015

Keywords:
Dengue virus
Non-structural protein NS4A
Amphipathic helix
Curvature sensing
NMR spectroscopy
Peptide membrane interaction

ABSTRACT

Dengue virus (DENV) infection is a growing public health threat with more than one-third of the world's population at risk. Non-structural protein 4A (NS4A), one of the least characterized viral proteins, is a highly hydrophobic transmembrane protein thought to induce the membrane alterations that harbor the viral replication complex. The NS4A N-terminal (amino acids 1–48), has been proposed to contain an amphipathic α-helix (AH). Mutations (L6E; M10E) designed to reduce the amphipathic character of the predicted AH, abolished viral replication and reduced NS4A oligomerization. Nuclear magnetic resonance (NMR) spectroscopy was used to characterize the N-terminal cytoplasmic region (amino acids 1–48) of both wild type and mutant NS4A in the presence of SDS micelles. Binding of the two N-terminal NS4A peptides to liposomes was studied as a function of membrane curvature and lipid composition. The NS4A N-terminal was found to contain two AHs separated by a non-helical linker. The above mentioned mutations did not significantly affect the helical secondary structure of this domain. However, they reduced the affinity of the N-terminal NS4A domain for lipid membranes. Binding of wild type NS4A(1–48) to liposomes is highly dependent on membrane curvature.

© 2015 Elsevier B.V. All rights reserved.

1. Introduction

Dengue virus (DENV) is an enveloped, positive sense single-stranded RNA virus that belongs to the *Flaviviridae*, a family that includes other major pathogens. The mosquito-borne DENV is the causative agent of dengue fever, the most rapidly spreading arboviral disease in humans [1].

After entering the host cell via endocytic pathways [2], the viral RNA is translated into a single polyprotein which is then processed by cellular and viral proteases to produce the structural capsid (C), premembrane (prM) and envelope (E) proteins and the non-structural (NS) proteins NS1, NS2A, NS2B, NS3, NS4A, NS4B, and NS5 [3]. In contrast to the structural proteins, NS proteins, are not a part of the mature DENV particle, however most of them were shown to be involved in viral replication.

DENV RNA synthesis occurs within replication complexes containing essential NS proteins, such as NS5 the viral RNA-dependent RNA polymerase, the viral RNA and host cell factors [4]. The replication complexes are located within a virus-induced and endoplasmic reticulum (ER)-derived complex membrane network [5,6] consisting of interconnected lipid vesicles and convoluted membranes [7]. NS4A localizes to the DENV replication complex and was found to be sufficient to induce host membrane alterations resembling the virus-induced membrane rearrangements [3].

NS4A is a hydrophobic 16 kDa transmembrane protein containing four predicted transmembrane segments (pTMSs) [3]. The C-terminal pTMS, also known as the 2 K fragment, is a signal peptide for the ER localization of NS4B and is not part of the mature NS4A [8]. Experimental evidence shows that the predicted TMS1 and 3 indeed span the membrane. In contrast, pTMS2 does not span the membrane and is thought to be imbedded in the luminal side of the ER membrane [3]. It is still unknown, how NS4A contributes to the substantial membrane deformations that are required to form the membrane scaffold for replication complex assembly.

Different mechanisms have been described by which proteins can remodel cellular membranes [9,10]. Insertion of amphipathic α-helices

Abbreviations: AH, amphipathic α-helix; CD, circular dichroism; DENV, dengue virus; DLS, dynamic light scattering; ER, endoplasmic reticulum; HCV, hepatitis C virus; NMR, nuclear magnetic resonance; NOE, nuclear overhauser effect; NS4A, non-structural protein 4A; NS4A(1–48), amino acids 1 to 48 of NS4A; pTMS, predicted transmembrane segment; RCI, random coil index; RU, response units; SPR, surface plasmon resonance; SUV, small unilamellar vesicle; TLC, thin layer chromatography

* Corresponding author at: Institute of Complex Systems, Structural Biochemistry (ICS-6), Forschungszentrum Jülich, 52425 Jülich, Germany. Tel.: +49 2461 615 385; fax: +49 2461 612 023.
E-mail address: b.koenig@fz-juelich.de (B.W. Koenig).
[1] Present address: Nestlé France, Atrium RDC, 7 Boulevard Pierre Carle, 77186 Noisiel, France.
[2] Present address: Department of Chemistry, University of Illinois at Chicago, 845 West Taylor Street, Chicago, IL 60607, United States.

http://dx.doi.org/10.1016/j.bbamem.2015.01.015
0005-2736/© 2015 Elsevier B.V. All rights reserved.

(AHs) into membranes is one of them. Embedding the hydrophobic face of the AH into one leaflet of a bilayer causes asymmetry that can induce local membrane curvature. Membrane curvature could also arise from asymmetrically shaped integral membrane proteins or complexes, and from oligomerization of membrane-bound proteins in or above the polar lipid water interface [10]. A single membrane altering protein may use more than one of these mechanisms to exert its activities [10].

Some AHs act as membrane curvature sensors. They bind membranes in a curvature sensitive manner, which is important for membrane curvature-dependent assembly or disassembly of protein complexes and for vesicular transport [11].

AHs identified in various viral proteins were found to be essential for viral replication, including hepatitis C virus (HCV) NS5A [12,13] and NS4B [14–16] and Semliki forest virus nsP1 [17]. AHs in viral proteins have been implicated in anchoring some of these non-structural proteins to the membrane. It was speculated, that these AHs could also be involved in the remodeling of intracellular membranes to form the complex membrane structures that harbor the viral replication complexes [4].

Secondary structure prediction indicates that the conformation of the N-terminal amino acids 1–48 of NS4A should be dominated by α-helices [18]. Furthermore, if the peptide would indeed form a regular α-helix, 18 amino acid residue stretches in the N-terminal half of this helix would have a significant amphipathic character with hydrophobic moments ranging from 0.3 to 0.4 (analyzed by Heliquest [19] based on the hydrophobicity scale of Fauchere and Pliska [20]). Helices with hydrophobic moments above 0.6 are considered highly amphipathic [19].

To examine the functional relevance of AH formation, mutations were introduced into the N-terminal region of NS4A with the aim to preserve the tendency to form an α-helix, but reduce the hydrophobic moment of the putative helix in amino acids 3–20 [18]. When inserted in the context of a DENV reporter replicon these NS4A mutations (L6E; M10E) abolished viral replication. These mutations also reduced homo-oligomerization of NS4A, but did not affect its localization [18]. Apparently, the N-terminal cytoplasmic domain of NS4A is crucial for DENV replication. However, its exact role is still unclear. In contrast to other viral proteins such as NS5A from the related hepatitis C virus where the AH presents the sole membrane anchor [12], DENV NS4A is a transmembrane protein [3]. Thus it is unlikely that the AH of NS4A serves as a primary membrane anchor. The fact that the mentioned AH mutations affect the oligomerization of NS4A supports a possible role of this domain in the induction of membrane curvature.

Experimental data on the three-dimensional structure of the NS4A cytoplasmic N-terminal domain and on its interaction with membranes are required in order to better understand the role of this domain in viral replication. Structural analysis could assist in answering the fundamental question if part of the N-terminal domain of wild type NS4A indeed forms an amphipathic helix and in assessing the structural consequences of the two introduced mutations.

Previous circular dichroism (CD) data had indicated that about 40% of the amino acids of both wild type and mutant NS4A (amino acids 1–48) peptides are located in α-helices in the presence of membrane mimicking micelles [18]. However, the CD data did not provide the sequence location and extension of these helices. In order to address these questions peptides corresponding to the N-terminal domain (amino acids 1–48) of wild type and mutant NS4A were recombinantly produced. These two peptides were analyzed in membrane mimicking micelles using liquid state NMR spectroscopy. CD and surface plasmon resonance (SPR) experiments were used to study the interaction of wild type and mutant NS4A (amino acids 1–48) peptides with liposomes resembling the lipid composition of human ER membranes and to test the influence of membrane curvature on the peptide membrane interaction.

2. Materials and methods

2.1. Recombinant protein production

A peptide (SLTLNLITEM GRLPTFMTQK ARDALDNLAV LHTAEAGGRA YNHALSEL) corresponding to the N-terminal 48 amino acid residues of the non-structural protein NS4A of dengue virus serotype 2 (NCBI Protein database accession number: NP739588) and a mutant version of this peptide was recombinantly produced in *Escherichia coli* BL21 cells. The peptides were expressed as fusion proteins with a double tag (GST and GB1 domains) preceding the amino acid sequence of the peptide as described [21]. The double tag was removed by enzymatic cleavage using TEV protease, resulting in an N-terminal serine in the produced peptides. This serine matches the N-terminal amino acid of DENV NS4A, i.e., the studied peptides do not contain any additional residues. Uniform isotope labeling with ^{15}N or ^{13}C, ^{15}N was achieved by expression in M9 medium containing ^{15}N ammonium chloride and ^{13}C glucose (Eurisotop, Saarbrücken, Germany) as the sole source of nitrogen and carbon, respectively. Unlabeled peptides were expressed in LB medium. The mutant peptide NS4A(1–48, L6E; M10E) carries two point mutations: L6E and M10E.

2.2. Lipids

Lipids were all purchased in chloroform solution from Avanti Polar Lipids (Alabaster, AL, USA) including: 1-palmitoyl-2-oleoyl-*sn*-glycero-3-phosphocholine (POPC); 1-palmitoyl-2-oleoyl-*sn*-glycero-3-phosphoethanolamine (POPE); 1,2-dioleoyl-*sn*-glycero-3-phospho-L-serine (sodium salt) (DOPS); L-α-phosphatidylinositol of bovine liver (sodium salt) (PI); sphingomyelin from chicken egg (SM); L-α-phosphatidic acid from chicken egg (sodium salt) (PA); and cardiolipin of bovine heart (sodium salt) (CL). Cholesterol (>99%) powder (Sigma-Aldrich, Taufkirchen, Germany) was dissolved in chloroform at 10 mg mL^{-1}.

Besides single component POPC membranes we studied two lipid mixtures: a POPC/DOPS mixture at a molar ratio of 4:1 and a multicomponent mixture resembling the composition of membranes in the ER [22]. A synthetic ER lipid mix with the following components was used: POPC/bovine heart CL/bovine liver PI/POPE/DOPS/chicken egg PA/chicken egg SM/cholesterol with molar ratios of 59:0.37:7.7:18:3.1:1.2:3.4:7.8.

2.3. Nuclear magnetic resonance

NMR samples contained 1 mM [*U*-^{15}N]- or [*U*-^{15}N, ^{13}C]-labeled NS4A(1–48) or NS4A(1–48, L6E; M10E) in 50 mM sodium phosphate buffer (pH 6.8), 10% (v/v) deuterium oxide, 0.03% (w/v) NaN_3, with or without 100 mM perdeuterated sodium dodecyl sulfate (SDS-d_{25}). SDS-d_{25} and ^2H_2O were obtained from Eurisotop.

NMR experiments were performed at 30 °C on Varian Unity INOVA, VNMRS and Bruker Avance III HD NMR instruments, equipped with cryogenic Z-axis pulse-field-gradient (PFG) triple resonance probes operating at proton frequencies of 600, 800, and 900 MHz.

Resonance assignment of protein backbone was accomplished using a combined set of heteronuclear multidimensional NMR experiments: 2D (^1H-^{15}N)-HSQC [23,24], 2D (^1H-^{15}N)-BEST-TROSY (BT) correlation [25], 2D (^1H-^{13}C)-HSQC [26], 3D HNCACB [27], 3D BT-HNCACB [28], 3D HNCO [29], 3D BT-HNCO [28], and 3D HNHA [30]. ^1H and ^{13}C chemical shifts were referenced directly to internal DSS at 0 ppm and ^{15}N chemical shifts were referenced indirectly to DSS using the absolute ratio of the ^{15}N and ^1H zero point frequencies [31]. NMR data were processed using NMRPipe, v.8.1 [32] and evaluated with CcpNmr v.2.3 [33] and TALOS-N software [34].

Heteronuclear {^1H}-^{15}N NOEs (nuclear overhauser effects) were derived from 2D spectra recorded at 18.8 T with or without 6 s of proton saturation [35]. The heteronuclear NOE is the ratio of the integral peak intensities of a given ^1H-^{15}N correlation measured with and without saturation, respectively.

2.4. Chemical shift-based analysis

The software program TALOS-N [34] predicts protein secondary structure from experimental protein backbone $^{13}C\alpha$, $^{13}C\beta$, $^{13}C'$, $^{1}H\alpha$, ^{15}N, and ^{1}HN NMR chemical shift data and database knowledge. TALOS-N classifies secondary structure either as helix (H), extended strand (E) or coil (L) [34]. In addition, TALOS-N provides insight into protein backbone dynamics based on the random coil index (RCI) method. An empirical correlation between the model-free backbone order parameter S^2 [36] and protein backbone secondary chemical shifts is exploited for deriving the order parameter RCI-S^2 [37,38].

2.5. Small unilamellar lipid vesicles (SUVs)

SUVs were prepared by extrusion or sonication using either a single lipid component or a synthetic mixture of different lipids. Appropriate volumes of the lipid chloroform stocks were transferred to a glass test tube at the desired molar ratios with a total amount of 5 mg of lipid per sample. Chloroform was removed by passing a gentle stream of nitrogen gas over the solution while slowly rotating the test tube, resulting in a thin film of lipid on the inner wall of the tube. High vacuum was applied for at least 3 h to remove chloroform traces. Lipid films were suspended under vortexing in 500 μL of sodium phosphate buffer (50 mM sodium phosphate, pH 6.8, 150 mM NaCl). Samples were subjected to three cycles of freezing and thawing in liquid nitrogen and a 60 °C water bath. Liposome solutions were passed 15 times or more through a nuclepore polycarbonate membrane with nominal pore diameter of either 30 or 50 nm (GE Healthcare, Freiburg, Germany) using a handheld LiposoFast Extruder (Avestin Europe, Mannheim, Germany) equipped with two 0.5 mL syringes. Sonicated lipid vesicles were produced starting from SUV solution obtained by extrusion through a 30 nm nuclepore membrane. Volumes of 500 μL per sample were transferred to 1.5 mL Eppendorf tubes, kept on ice and treated with a 3 mm microtip of a Branson 250 sonifier. Ten cycles of sonication (20 s) and intermediate cooling (2 min) were applied. Finally, the hydrodynamic radius of the liposomes was determined by dynamic light scattering. Liposomes were checked for lipid degradation products by thin layer chromatography (TLC) using Alugram SIL G sheets (Macherey-Nagel, Düren, Germany) and a mobile phase of chloroform, methanol, and aqueous ammonia (25%) in a volume ratio of 13:7:1.

2.6. Circular dichroism (CD)

CD data were measured with a Jasco J-1100 instrument (Jasco, Groß-Ulmstadt, Germany) at 30 °C using a QS quartz cell with optical path length of 1 mm (Hellma, Müllheim, Germany). All samples were prepared in 50 mM sodium phosphate buffer, pH 6.8, 150 mM NaCl. Appropriate amounts of extruded or sonicated liposome stock and buffer were supplemented with peptide stock to give a final lipid concentration of 10 mg mL^{-1}, i.e., about 13 mM, in all liposome samples. Additional samples contained peptide in buffer or micelles (100 mM SDS). Concentration of NS4A(1–48) or NS4A(1–48, L6E; M10E) peptides was 40 μM in all samples. Light scattering due to the large size of liposomes and light extinction due to high concentration of chloride ions limited acquisition of CD data to the wavelength range above 205 nm. CD data were recorded in continuous scan mode (scan speed 50 nm min^{-1}, bandwidth 1 nm, integration time constant 0.5 s, accumulation of 5 scans). Appropriate background spectra reflecting contributions from the buffer, liposome or detergent solution were subtracted from each curve.

2.7. Surface plasmon resonance (SPR)

SPR data were collected with a Biacore X instrument using L1 sensor chips (GE Healthcare, Freiburg, Germany). L1 chips were equilibrated with 50 mM sodium phosphate buffer pH 6.8 for 30 min and then stripped with short pulses (1 min at a flow rate of 20 μL min^{-1}) of 20 mM CHAPS (3-((3-cholamidopropyl)-dimethylammonio)-1-propane sulfonate). The entire flow path was washed with phosphate buffer. For liposome immobilization, the SUV solution (80 μL, with a nominal lipid concentration of 2 mg mL^{-1}, extruded through a 50 nm nuclepore membrane) was injected at a flow rate of 2 μL min^{-1}. Three short pulses of 50 mM NaOH were applied at 10 μL min^{-1} in order to remove loosely bound liposomes and to achieve a stable baseline. A solution of 0.1 mg mL^{-1} bovine serum albumin (BSA, Sigma-Aldrich) was injected for 1 min at a flow rate of 10 μL min^{-1} in order to block potential non-specific ligand binding sites on the surface. Initial blank injections with running buffer only and binding experiments with 30 μM of the NS4A peptide were performed at a flow rate of 20 μL min^{-1}. In the binding experiments the analyte solution was injected for 30 s (association phase) followed by buffer injection for 100 s or longer (dissociation phase). A corrected sensorgram was obtained by subtracting the sensorgram of the blank injection from that of the immediately following binding experiment. Complete return of the response (RU) signal to pre-injection level could not be achieved, neither by extending the running buffer injection times to several hours nor by established regeneration procedures such as high salt concentration or extreme pH buffers. Therefore, the L1 sensor chip was completely stripped of lipids and protein with repeated short pulses of 20 mM CHAPS until the RU value became similar to the original values. Stripping was repeated after every single binding experiment.

2.8. Dynamic light scattering (DLS)

Data were measured using the Dyna Pro instrument (Protein Solutions, Lakewood, NJ, USA) equipped with a 3 mm path length 45 μL quartz cell. Liposome solutions (10 mg of lipid per mL) were diluted 100-fold with buffer (50 mM sodium phosphate pH 6.8, 150 mM NaCl) directly after extrusion or sonication and measured immediately. Data were analyzed with Dynamics V6 software distributed with the instrument. Experimental data were fitted to the model of Rayleigh spheres.

3. Results

3.1. NMR backbone signal assignment

Both wild type and mutant NS4A(1–48) peptides were analyzed using liquid state NMR spectroscopy in the presence of 100 mM SDS-d_{25}. An almost complete backbone resonance assignment of the two peptides was accomplished. In total, 98% of the expected resonances of both NS4A(1–48) and NS4A(1–48, L6E; M10E) were identified. Resonance assignments for the two NS4A N-terminal peptides have been deposited at the Biological Magnetic Resonance Data Bank (BMRB) under accession numbers 25179 (wild type) and 25180 (mutant).

3.2. NMR-based secondary structure analysis

Highly resolved two-dimensional (^{1}H-^{15}N) correlation spectra were obtained for both wild type and mutant NS4A peptides in membrane mimicking SDS micelles (Fig. 1) and in detergent-free buffer at 30 °C. The low spectral dispersion and the occupied range of ^{1}HN chemical shifts in the NMR spectra of both peptides in buffer (see Fig. 7 in [21]) are in agreement with a random coil conformational ensemble, which was also suggested by earlier CD data [18]. Addition of SDS increases the spectral dispersion and causes a clear upfield shift, in particular in the proton dimension, for many of the observed cross-peaks, very likely indicating the formation of secondary structure elements.

The experimental data was used for secondary structure prediction employing the TALOS-N software package [34]. Fig. 2A displays the resulting chemical shift-based secondary structure prediction for the

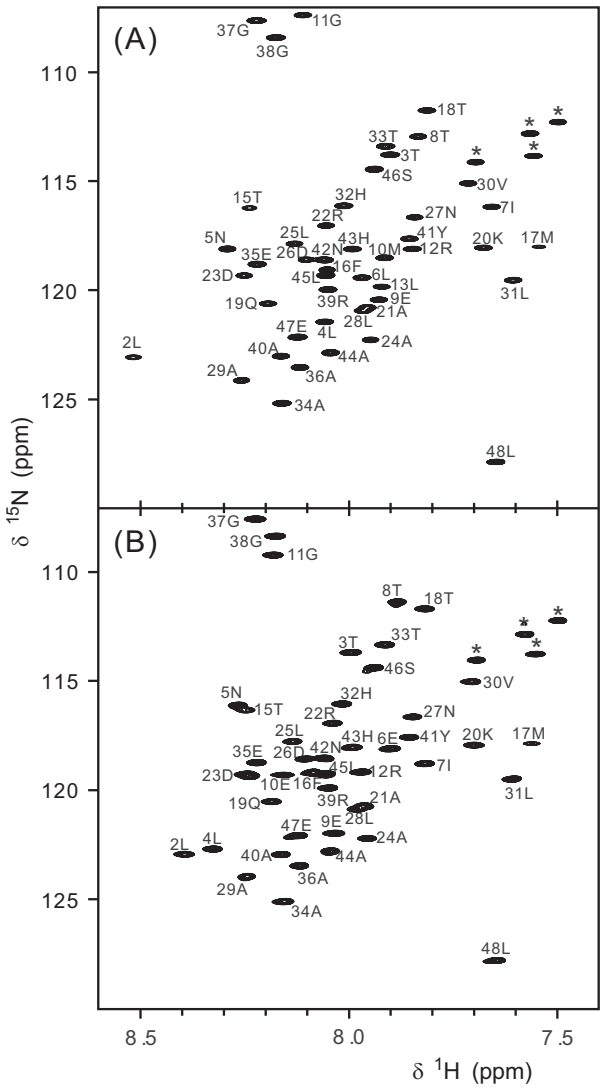

Fig. 1. (^{1}H-^{15}N)-HSQC spectra of [*U*-^{15}N]-labeled NS4A(1–48) (A) or NS4A(1–48, L6E; M10E) (B) in the presence of 100 mM SDS-d_{25}. All assigned backbone amide ^1H_N-^{15}N correlations are labeled with the corresponding amino acid sequence position and type (in one letter code). Side chain ^{1}H-^{15}N correlations are denoted by asterisks.

two NS4A peptides. Solid and open bars indicate amino acids with helical secondary structure in the wild type (residues 5-to-9 and 15-to-31) and mutant (residues 4-to-7 and 15-to-31) NS4A peptides in the presence of SDS micelles. The height of the bars reflects the probability of helical structure for the given residue. No indications for amino acid residues in extended strand conformations were found. Prediction was inconclusive for Pro14 (wild type) and for the N- and C-terminal residues. All remaining residues were assigned as "coil" by the program. Clearly, addition of SDS causes formation of two helical segments, designated helices 1 and 2, connected by an unstructured linker. This conformation occurred both in the wild type and mutant NS4A (1–48) peptides.

3.3. Backbone dynamics

RCI-S^2 values reported by TALOS-N and heteronuclear {^{1}H}-^{15}N-NOEs of the two NS4A peptides are presented in Fig. 2B and C, respectively. The model-free backbone order parameter S^2 [36] as well as {^{1}H}-^{15}N-NOE-ratios reflect protein dynamics on the pico- to nanosecond timescale [39]. The magnitude of the parameter values is sensitive to small scale conformational fluctuations. Rigid secondary structure elements are characterized by large RCI-S^2 above 0.85 [38] and large positive {^{1}H}-^{15}N-NOEs ratios around 0.8 [40], while flexible residues show significantly lower values. The data in Fig. 2 indicate a rather rigid α-helix 2 with slightly increased dynamics at the C-terminus of helix 2 in both peptides. Rapid internal motions become increasingly prominent in the following sequence: helix 1, interhelical linker, N- and C-terminus of the peptide.

3.4. Interaction of NS4A peptides with immobilized liposomes

In an attempt to further assess the role of the N-terminal of NS4A we previously determined its ability to bind membranes using SPR experiments [18]. Here SPR was used to further test the binding of NS4A(1–48) and NS4A(1–48, L6E; M10E) peptides to lipid bilayers modeling the lipid composition at the ER membrane [22].

Both the wild type and mutant peptides bound to the studied liposomes. Association and dissociation of the main fraction of peptides occurred on a rapid timescale, reflected by the fast rise and steep decline of the response signal that immediately followed the beginning and the end of analyte injection. Such fast dissociation is a characteristic of low stability complexes. The maximum response of wild type peptide was about sevenfold higher than that of the mutant (Fig. 3) indicating a higher affinity of the wild type peptide towards the membranes. Dissociation of the wild type peptide from the membranes was slower than that of the mutant peptide. Furthermore, the wild type peptide showed lipid-specific differences in the association and dissociation kinetics (Fig. 3A). Both processes were more rapid for NS4A(1–48) binding to POPC and slower for peptide binding to ER mix and POPC/DOPS membranes. It is conceivable, that peptide association to the liposomes involves different mechanisms or binding sites with different affinity and kinetics. The initial fast association and dissociation phases are apparently followed by slower rising and declining responses, respectively (Fig. 3). This behavior might be explained, for example, by peptide oligomerization that follows the initial rapid peptide binding to the liposome. During the dissociation phase a large fraction of the liposome-associated peptide is rapidly released, while some of the peptide molecules seem to be irreversibly bound. These empirical observations are more pronounced for the wild type peptide. The somewhat different height of the response signals during association of a given peptide to the three different membrane compositions studied (Fig. 3) are perhaps due to differences in the amount of liposomes immobilized on each of the three L1 chips and do not necessarily reflect differences in peptide affinity. In order to show that the SPR results are not due to non-specific direct binding of the peptide to the chip, 0.1 mg mL^{-1} BSA immobilization was used instead of liposomes. In these experiments, both NS4A peptides yielded responses lower than 20 RU. This observation confirms that the sensorgrams shown in Fig. 3 are not a result of non-specific interactions of the NS4A peptides with the L1 chip. Taken together these results suggest that the two point mutations reduce the strength of liposome binding and/or the homo-oligomerization tendency of the NS4A(1–48) peptide.

3.5. Interaction of NS4A peptides with liposomes

CD spectroscopy was used to monitor formation of helical secondary structure upon NS4A peptide interaction with liposomes of different lipid composition and surface curvature. CD spectra of α-helices show two characteristic minima at 208 and 222 nm. The depth of the minima increases with the helix content in the sample [41]. CD spectra of NS4A wild type (left) and mutant peptides (right) in various environments are presented in Fig. 4. CD data of NS4A peptides recorded in the presence of liposomes or micelles are population-weighted averages of the CD curves of free and bound peptide conformations in the corresponding sample. Both peptides display less than 10% helical structure

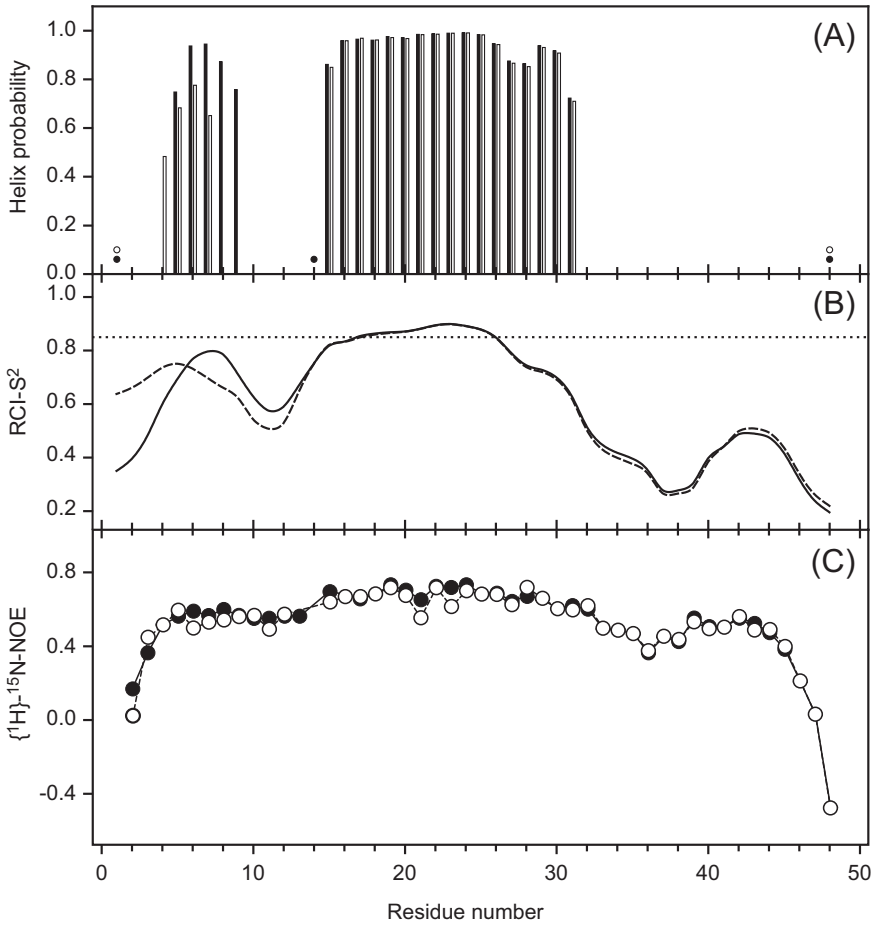

Fig. 2. Secondary structure prediction (A), RCI-based order parameter RCI-S^2 (B), and {^{1}H}-^{15}N heteronuclear NOE intensity ratios (C) for NS4A(1–48) (filled bars and circles in (A, C), solid line in (B)) and NS4A(1–48, L6E; M10E) (open bars and circles in (A, C), broken line in (B)) in buffer containing 100 mM SDS-d_{25}. Data shown in A and B are based on secondary chemical shifts and were provided by TALOS-N. Bars in panel A report residues with helical secondary structure. None of the residues was predicted to adopt an extended strand conformation. Circles indicate lack of prediction at the termini of the peptides or an inconclusive prediction in the case of P14 of the wild type sequence. All remaining amino acid residues were predicted as "coil". Predicted RCI-S^2 values (B) are connected by a cubic spline function. The dotted line indicates RCI-S^2 = 0.85.

in buffer (Fig. 4, dashed black line) but the α-helix content increases to about 36% (wild type) and 30% (mutant) upon addition of 100 mM SDS (Fig. 4, solid black line) [18].

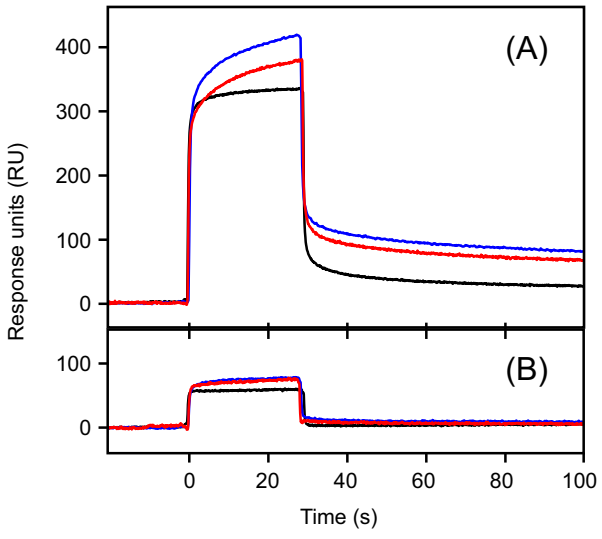

Fig. 3. Surface plasmon resonance sensorgrams reflecting the interaction of NS4A wild type (A) and mutant peptide (B) with immobilized liposomes composed of POPC (black); POPC/DOPS (4:1) (blue), and a mix of lipids resembling human ER membranes (red). Peptide injection started at time 0 s and lasted for 30 s.

Addition of extruded liposomes (hydrodynamic radius r_h = 33 nm) consisting of either POPC, POPC/DOPS (4:1), or a synthetic ER lipid mix, respectively, to a final concentration of about 13 mM lipid (10 mg mL^{-1}) resulted in an increase in the helicity of the wild type peptide, but did not significantly affect the mutant CD data (Fig. 4, blue). Almost identical but more noisy CD curves were obtained when using extruded liposomes at the same lipid concentration but with r_h = 48 nm instead of 33 nm (data not shown). When sonicated liposomes (r_h = 26 nm) instead of extruded ones were added at the same lipid concentration (Fig. 4, red), higher helix content is found in the wild type peptide samples. Only marginal changes occur with the mutant peptide.

CD curves of wild type NS4A peptide in the presence of SDS micelles or either one of the three differently composed, sonicated liposomes display high similarity (Fig. 4A, C and E). A possible interpretation of the almost matching CD curves is a similar conformation and a similar fraction of bound NS4A peptide in all four samples. If we further assume that NS4A(1–48) binds all types of liposomes in an identical conformation, then it becomes clear from Fig. 4 that a significantly smaller fraction of NS4A(1–48) binds to the larger (extruded) liposomes in comparison to smaller (sonicated) ones. Apparently, NS4A(1–48) binding to liposomes is sensitive to membrane curvature and shows a steep dependence on liposome size when r_h is close to 30 nm. The difference in the lipid composition of the membranes used for the CD measurements shown in Fig. 4 does not have a strong influence on NS4A peptide binding. The mutant NS4A peptide shows no increase in helical secondary structure upon addition of either extruded or

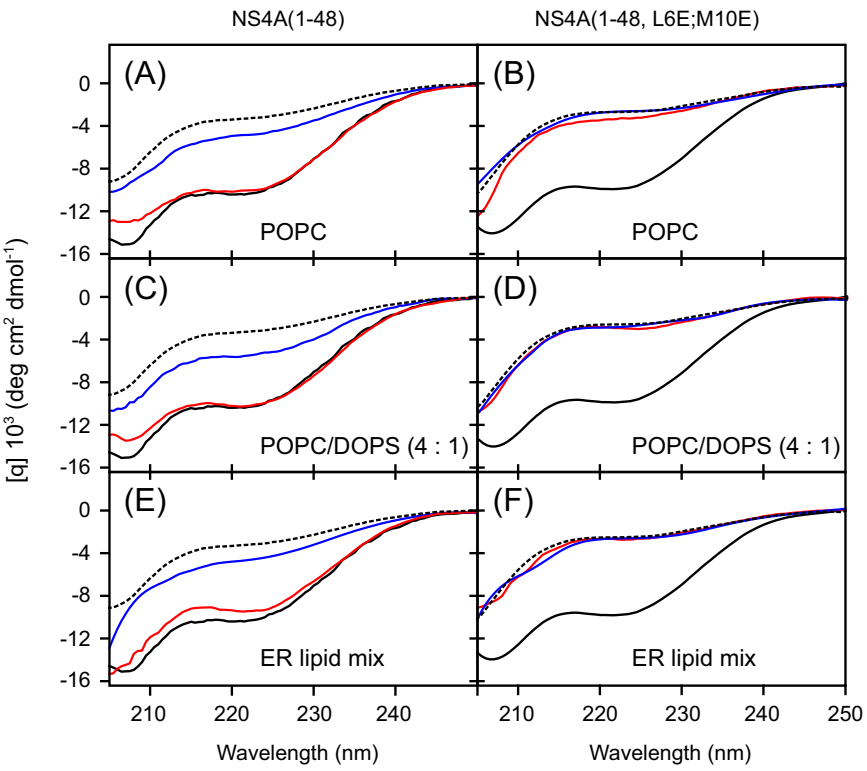

Fig. 4. Mean residue ellipticity of NS4A wild type (left) and mutant peptides (right) in the presence of liposomes (10 mg lipid per mL) prepared from POPC (A, B); POPC/DOPS (4:1) (C, D); and a mix of lipids resembling the lipid composition of human ER membranes (E, F). Liposomes were produced by extrusion (blue) or by sonication (red). CD spectra of the peptides in phosphate buffer (black, dashed line) and in micelle solution (100 mM SDS, black) have been added for comparison. Peptide concentration was 40 μM in all samples.

sonicated liposomes at the lipid and peptide concentrations used in these experiments.

4. Discussion

4.1. Implications of the NS4A peptide structure

We conducted the first characterization of the three-dimensional structure and dynamics of the N-terminal 48 amino acid peptide of DENV NS4A protein in membrane mimicking micelles. The amino acid sequence of NS4A(1–48) shows an intrinsic bias for α-helix formation. Application of multiple secondary structure prediction algorithms results in a consensus structure with three helices, encompassing residues 4–10, 15–35, and 40–47 of NS4A(1–48) [18]. In the case of the NS4A mutant peptide, different algorithms strongly disagree on length and position of the most N-terminal helix. Very little, if any secondary structure was experimentally detected for the NS4A peptides in aqueous buffer devoid of membranes and detergent micelles. Addition of membrane mimicking SDS micelles induced formation of two helices in each of the peptides. The predicted N-terminal helix 1 in the wild type peptide almost matches the NMR data. The experimentally determined helix 2 (amino acid residues 15–31) is slightly shorter than the prediction (residues 15–35). The third predicted helix could not be experimentally confirmed under the conditions used.

Helices 1 and 2 were found to be connected via an unstructured linker. Reduced RCI-S^2 values of the amino acid residues in the linker (Fig. 2B) indicate higher dynamics in comparison to the helices. According to our results the starting point of helix 2 is Tyr15. Interestingly, the preceding residue is a proline (Pro14). Proline has the lowest helix propensity among all 20 naturally occurring amino acids due to both its unique geometry and the lack of an amide hydrogen required for helix stabilizing hydrogen bonding [42]. The relatively few proline residues found in the interior of α-helices cause a disruption or a kink of the helix because steric restrictions prevent proline from forming canonical α-helical geometry [43]. Mutation of Pro14 to alanine in the context of a DENV reporter replicon abolished viral replication [18]. This mutation may cause an N-terminal extension of α-helix 2, since alanine is the amino acid with highest helix propensity [42]. It is conceivable that the separation of helices 1 and 2 by a flexible linker or at least a kink is a crucial requirement for functional interaction of NS4A with membranes and/or proteins. Interestingly, a recent study showed that a specific interaction between the N-terminal of NS4A (amino acids 1–50) and cytoskeleton protein vimentin is crucial for correct regulation of DENV replication complex construction [44], indicating that this idea is feasible.

The observed helices display an amphipathic character. A regular α-helix formed by NS4A amino acid residues 15–31 (helix 2) has a moderate hydrophobic moment $<\mu_h>$ of 0.287 (http://heliquest.ipmc.cnrs.fr) [19]. However, the central 13 amino acid residues of this α-helix display a very strongly amphipathic character ($<\mu_h> = 0.512$). Helical wheel plots of the very short helix 1 of wild type and mutant NS4A, respectively, reveal distinct polar and hydrophobic faces, too. However, the two mutations of hydrophobic amino acids Leu6 and Met10 to anionic glutamate cause a counterclockwise rotation of the hydrophobic face of this short helix by ~45°, perhaps explaining the observed shift of helix 1 by one residue along the sequence. Acknowledging the amphipathic character of the experimentally identified helices 1 and 2, they will be referred to as AH1 and AH2 of dengue virus protein NS4A in what follows.

Dengue virus carrying the two mutations L6E and M10E in the NS4A protein is replication-deficient. However, the structural consequences of the two mutations are rather small in the micelle bound peptide and appear to be limited to the N-terminal AH1, which includes one and is very close to the second mutation site. Most likely, AH1 extends from Asn5 to Glu9 in wild type NS4A(1–48) and from Leu4 to Ile7 in the mutant. In addition to its apparent shift by one residue towards the N-terminus, helix 1 of the mutant shows a lower helix probability for the individual amino acid residues and has lower order parameters indicating increased conformational fluctuations in comparison to the

wild type sequence (Fig. 2A, B). Taken together these small changes may reflect a reduced free energy gain upon micelle binding of the mutant as compared to the wild type peptide. Nevertheless, at the high concentration of potential peptide binding sites present at 100 mM SDS, a large fraction of both wild type and mutant peptide binds and shows α-helix formation. The dramatically different amounts of helical conformation observed in the wild type vs. mutant peptide upon addition of liposomes (cf. Fig. 4) are perhaps caused by a reduced membrane affinity of the mutant in comparison with the wild type peptide.

Putative AH forming peptides are often unstructured in aqueous buffer while addition of liposomes or detergent micelles induces helix formation. SDS micelles and lipid bilayers both have a polar head group water interface and a hydrophobic interior. Differences between the two membrane mimics include the nature of the head groups and hydrocarbon chains as well as the surface curvature. Micelles are highly dynamic with continuous exchange of detergent molecules between the monomeric and micellar state. NMR provides a detailed characterization of the structure and dynamics of micelle-bound peptide. However, membrane- and micelle-bound peptide conformations are not necessarily identical. Similar CD data of the wild type NS4A peptide in SDS micelles and sonicated liposomes (Fig. 4) are merely an argument for similar structures of the bound peptide in both systems. The experimentally determined structure of NS4A(1–48) in SDS micelles serves as a hypothetical model of the membrane-bound peptide structure.

4.2. NS4A(1–48) binds preferentially to highly curved liposomes

A protein might bind to a membrane without undergoing a conformational change. On the other hand, the increase of helical secondary structure of the wild type NS4A(1–48) observed upon addition of liposomes clearly indicates binding. Assuming a partially helical membrane-bound and an almost random coil unbound NS4A(1–48) conformation, we can use the degree of helicity reflected in the CD curves of wild type NS4A(1–48) as an indicator of peptide binding to liposomes. The CD data in Fig. 4 suggest preferential binding of NS4A(1–48) to the convex face of highly curved lipid membranes. Insertion of hydrophobic amino acid side chains into tightly packed membranes is energetically less favorable than intercalation into existing lipid bilayer packing defects. Such defects are abundant in the strained outer leaflet of small liposomes and have been implicated in curvature-dependent binding of a number of AH motifs to membranes [11,45,46].

The L6E; M10E mutations reduced the affinity of the N-terminal NS4A peptide for immobilized liposomes (Fig. 3) and virtually abandoned helix formation upon addition of all liposome types tested in the CD experiments (Fig. 4). Variation of the lipid composition had only small effects on the interaction of NS4A(1–48) with liposomes in comparison to the introduction of mutations (L6E; M10E) or the influence of membrane curvature (Figs. 3 and 4). Exploration of the more subtle effects of membrane composition will require additional systematic and quantitative studies.

4.3. Potential role of curvature sensing motif in NS4A(1–48)

NS4A localizes to the ER and to virus-induced ER-derived membranes. Individual expression of DENV NS4A lacking the 2 K fragment was previously shown to be sufficient to induce comparable membrane alterations [3]. Our results may suggest a role for NS4A in the formation of highly curved membrane entities. Such entities occurring during DENV replication were previously described as vesicular structures that are ~80 to 90 nm in diameter. These vesicles show tubular connections to the cytoplasm with a radius of ~10 nm [7,47]. The N-terminus of NS4A maps to the cytoplasmic side, i.e., the inner side of these structures. Both spherical vesicles and tubules are concave on the inner side. However, a more complex, saddle-shaped geometry with both negative and positive curvature occurs in neck regions connecting vesicles and tubules [9]. The vesicular structures are thought to develop from invaginations of the ER membrane. Recent molecular dynamics simulations on a NS4A model encompassing the membrane spanning domains pTMS1 and pTMS3 as well as the membrane-associated domain pTMS2 indicate, that this NS4A model induces membrane undulation and local bending with a radius comparable to the reported vesicular structures [47]. The N-terminal region of NS4A inclusive of AH1 and AH2 was not part of the NS4A model studied by Lin et al. [47]. These AHs may drive the protein into convex regions of the undulated ER membrane where the protein could accumulate, oligomerize, or participate in complex formation and perhaps induce or support formation of the vesicle neck. Energetically favorable insertion of hydrophobic amino acid side chains into existing defects in the cytoplasmic leaflet of locally bend ER membranes could stabilize existing curvature of the membrane while subsequent NS4A oligomerization or complex formation in or on the membrane may increase, modify or induce local curvature. This, of course, is a highly speculative model that should be further confirmed by additional experimental evidence.

In summary, we provide the first characterization of the three dimensional structure of the N-terminal of NS4A, a central protein in the life cycle of DENV. The NS4A N-terminal was found to contain two AHs separated by an unstructured linker in the presence of SDS micelles. The NS4A(1–48) peptide binds to liposomes in a membrane curvature-dependent manner. The double mutation L6E and M10E in the NS4A sequence abandons DENV replication in a replicon system [18]. The same two mutations strongly reduce lipid membrane binding. The two AHs in the N-terminus of NS4A may be crucial for membrane binding, curvature sensing and perhaps curvature stabilization.

Transparency document

The Transparency document associated with this article can be found, in the online version.

Acknowledgments

We thank Omer Stern and Julian Glück for fruitful discussions. D. W. received funding from the DFG within the SFB 947. D. W. received funding from and Y.-F. H. was a scholarship holder of the Graduate School Molecules of Infection (MOI), funded by the Jürgen Manchot Foundation.

References

[1] S. Bhatt, P.W. Gething, O.J. Brady, J.P. Messina, A.W. Farlow, C.L. Moyes, J.M. Drake, J.S. Brownstein, A.G. Hoen, O. Sankoh, M.F. Myers, D.B. George, T. Jaenisch, G.R. Wint, C.P. Simmons, T.W. Scott, J.J. Farrar, S.I. Hay, The global distribution and burden of dengue, Nature 496 (2013) 504–507.
[2] E.G. Acosta, V. Castilla, E.B. Damonte, Alternative infectious entry pathways for dengue virus serotypes into mammalian cells, Cell. Microbiol. 11 (2009) 1533–1549.
[3] S. Miller, S. Kastner, J. Krijnse-Locker, S. Buhler, R. Bartenschlager, The non-structural protein 4A of dengue virus is an integral membrane protein inducing membrane alterations in a 2K-regulated manner, J. Biol. Chem. 282 (2007) 8873–8882.
[4] S. Miller, J. Krijnse-Locker, Modification of intracellular membrane structures for virus replication, Nat. Rev. Microbiol. 6 (2008) 363–374.
[5] A. Salonen, T. Ahola, L. Kaariainen, Viral RNA replication in association with cellular membranes, Curr. Top. Microbiol. Immunol. 285 (2005) 139–173.
[6] J. Mackenzie, Wrapping things up about virus RNA replication, Traffic 6 (2005) 967–977.
[7] S. Welsch, S. Miller, I. Romero-Brey, A. Merz, C.K.E. Bleck, P. Walther, S.D. Fuller, C. Antony, J. Krijnse-Locker, R. Bartenschlager, Composition and three-dimensional architecture of the dengue virus replication and assembly sites, Cell Host Microbe 5 (2009) 365–375.
[8] C. Lin, S.M. Amberg, T.J. Chambers, C.M. Rice, Cleavage at a novel site in the NS4A region by the yellow fever virus NS2B-3 proteinase is a prerequisite for processing at the downstream 4A/4B signalase site, J. Virol. 67 (1993) 2327–2335.
[9] J. Zimmerberg, M.M. Kozlov, How proteins produce cellular membrane curvature, Nat. Rev. Mol. Cell Biol. 7 (2006) 9–19.
[10] H.T. McMahon, J.L. Gallop, Membrane curvature and mechanisms of dynamic cell membrane remodelling, Nature 438 (2005) 590–596.
[11] G. Drin, B. Antonny, Amphipathic helices and membrane curvature, FEBS Lett. 584 (2010) 1840–1847.
[12] V. Brass, E. Bieck, R. Montserret, B. Wolk, J.A. Hellings, H.E. Blum, F. Penin, D. Moradpour, An amino-terminal amphipathic alpha-helix mediates membrane

association of the hepatitis C virus nonstructural protein 5A, J. Biol. Chem. 277 (2002) 8130–8139.
[13] M. Elazar, K.H. Cheong, P. Liu, H.B. Greenberg, C.M. Rice, J.S. Glenn, Amphipathic helix-dependent localization of NS5A mediates hepatitis C virus RNA replication, J. Virol. 77 (2003) 6055–6061.
[14] M. Elazar, P. Liu, C.M. Rice, J.S. Glenn, An N-terminal amphipathic helix in hepatitis C virus (HCV) NS4B mediates membrane association, correct localization of replication complex proteins, and HCV RNA replication, J. Virol. 78 (2004) 11393–11400.
[15] J. Gouttenoire, V. Castet, R. Montserret, N. Arora, V. Raussens, J.M. Ruysschaert, E. Diesis, H.E. Blum, F. Penin, D. Moradpour, Identification of a novel determinant for membrane association in hepatitis C Virus nonstructural protein 4B, J. Virol. 83 (2009) 6257–6268.
[16] N.J. Cho, H. Dvory-Sobol, C. Lee, S.J. Cho, P. Bryson, M. Masek, M. Elazar, C.W. Frank, J.S. Glenn, Identification of a class of HCV inhibitors directed against the nonstructural protein NS4B, Sci. Transl. Med. 2 (2010).
[17] P. Spuul, A. Salonen, A. Merits, E. Jokitalo, L. Kaariainen, T. Ahola, Role of the amphipathic peptide of Semliki forest virus replicase protein nsP1 in membrane association and virus replication, J. Virol. 81 (2007) 872–883.
[18] O. Stern, Y.F. Hung, O. Valdau, Y. Yaffe, E. Harris, S. Hoffmann, D. Willbold, E.H. Sklan, An N-terminal amphipathic helix in dengue virus nonstructural protein 4A mediates oligomerization and is essential for replication, J. Virol. 87 (2013) 4080–4085.
[19] R. Gautier, D. Douguet, B. Antonny, G. Drin, HELIQUEST: a web server to screen sequences with specific alpha-helical properties, Bioinformatics 24 (2008) 2101–2102.
[20] J.L. Fauchere, V. Pliska, Hydrophobic parameters-Pi of amino-acid side-chains from the partitioning of N-acetyl-amino-acid amides, Eur. J. Med. Chem. 18 (1983) 369–375.
[21] Y.F. Hung, O. Valdau, S. Schunke, O. Stern, B.W. Koenig, D. Willbold, S. Hoffmann, Recombinant production of the amino terminal cytoplasmic region of dengue virus non-structural protein 4A for structural studies, PLoS One 9 (2014) e86482.
[22] H. Nemesio, F. Palomares-Jerez, J. Villalain, NS4A and NS4B proteins from dengue virus: membranotropic regions, Biochim. Biophys. Acta 1818 (2012) 2818–2830.
[23] G. Bodenhausen, D.J. Ruben, Natural abundance nitrogen-15 NMR by enhanced heteronuclear spectroscopy, Chem. Phys. Lett. 69 (1980) 185–189.
[24] S. Grzesiek, A. Bax, Amino acid type determination in the sequential assignment procedure of uniformly 13C/15 N-enriched proteins, J. Biomol. NMR 3 (1993) 185–204.
[25] A. Favier, B. Brutscher, Recovering lost magnetization: polarization enhancement in biomolecular NMR, J. Biomol. NMR 49 (2011) 9–15.
[26] L.E. Kay, P. Keifer, T. Saarinen, Pure absorption gradient enhanced heteronuclear single quantum correlation spectroscopy with improved sensitivity, J. Am. Chem. Soc. 114 (1992) 10663–10665.
[27] M. Wittekind, L. Mueller, HNCACB, a high-sensitivity 3D NMR experiment to correlate amide-proton and nitrogen resonances with the alpha- and beta-carbon resonances in proteins, J. Magn. Reson. Ser. B 101 (1993) 201–205.
[28] Z. Solyom, M. Schwarten, L. Geist, R. Konrat, D. Willbold, B. Brutscher, BEST-TROSY experiments for time-efficient sequential resonance assignment of large disordered proteins, J. Biomol. NMR 55 (2013) 311–321.
[29] M. Ikura, L.E. Kay, A. Bax, A novel approach for sequential assignment of 1H, 13C, and 15N spectra of proteins: heteronuclear triple-resonance three-dimensional NMR spectroscopy. Application to calmodulin, Biochemistry 29 (1990) 4659–4667.
[30] G.W. Vuister, A. Bax, Quantitative J correlation: a new approach for measuring homonuclear three-bond $J(H_N\text{-}H\alpha)$ coupling constants in ^{15}N-enriched proteins, J. Am. Chem. Soc. 115 (1993) 7772–7777.
[31] D.S. Wishart, C.G. Bigam, A. Holm, R.S. Hodges, B.D. Sykes, 1H, 13C and 15N random coil NMR chemical shifts of the common amino acids. I. Investigations of nearest-neighbor effects, J. Biomol. NMR 5 (1995) 67–81.
[32] F. Delaglio, S. Grzesiek, G.W. Vuister, G. Zhu, J. Pfeifer, A. Bax, NMRPipe: a multidimensional spectral processing system based on UNIX pipes, J. Biomol. NMR 6 (1995) 277–293.
[33] W.F. Vranken, W. Boucher, T.J. Stevens, R.H. Fogh, A. Pajon, M. Llinas, E.L. Ulrich, J.L. Markley, J. Ionides, E.D. Laue, The CCPN data model for NMR spectroscopy: development of a software pipeline, Proteins 59 (2005) 687–696.
[34] Y. Shen, A. Bax, Protein backbone and sidechain torsion angles predicted from NMR chemical shifts using artificial neural networks, J. Biomol. NMR 56 (2013) 227–241.
[35] N.A. Farrow, R. Muhandiram, A.U. Singer, S.M. Pascal, C.M. Kay, G. Gish, S.E. Shoelson, T. Pawson, J.D. Forman-Kay, L.E. Kay, Backbone dynamics of a free and phosphopeptide-complexed Src homology 2 domain studied by 15N NMR relaxation, Biochemistry 33 (1994) 5984–6003.
[36] G. Lipari, A. Szabo, Model-free approach to the interpretation of nuclear magnetic resonance relaxation in macromolecules. 1. Theory and range of validity, J. Am. Chem. Soc. 104 (1982) 4546–4559.
[37] M.V. Berjanskii, D.S. Wishart, A simple method to predict protein flexibility using secondary chemical shifts, J. Am. Chem. Soc. 127 (2005) 14970–14971.
[38] M.V. Berjanskii, D.S. Wishart, Application of the random coil index to studying protein flexibility, J. Biomol. NMR 40 (2008) 31–48.
[39] L. Salmon, G. Bouvignies, P. Markwick, M. Blackledge, Nuclear Magnetic Resonance provides a quantitative description of protein conformational flexibility on physiologically important time scales, Biochemistry 50 (2011) 2735–2747.
[40] L.E. Kay, D.A. Torchia, A. Bax, Backbone dynamics of proteins as studied by 15N inverse detected heteronuclear NMR spectroscopy: application to staphylococcal nuclease, Biochemistry 28 (1989) 8972–8979.
[41] N. Greenfield, G.D. Fasman, Computed circular dichroism spectra for the evaluation of protein conformation, Biochemistry 8 (1969) 4108–4116.
[42] C.N. Pace, J.M. Scholtz, A helix propensity scale based on experimental studies of peptides and proteins, Biophys. J. 75 (1998) 422–427.
[43] H.R. Wilman, J. Shi, C.M. Deane, Helix kinks are equally prevalent in soluble and membrane proteins, Proteins 82 (2014) 1960–1970.
[44] C.S. Teo, J.J. Chu, Cellular vimentin regulates construction of dengue virus replication complexes through interaction with NS4A protein, J. Virol. 88 (2014) 1897–1913.
[45] G. Drin, J.F. Casella, R. Gautier, T. Boehmer, T.U. Schwartz, B. Antonny, A general amphipathic alpha-helical motif for sensing membrane curvature, Nat. Struct. Mol. Biol. 14 (2007) 138–146.
[46] N.S. Hatzakis, V.K. Bhatia, J. Larsen, K.L. Madsen, P.Y. Bolinger, A.H. Kunding, J. Castillo, U. Gether, P. Hedegard, D. Stamou, How curved membranes recruit amphipathic helices and protein anchoring motifs, Nat. Chem. Biol. 5 (2009) 835–841.
[47] M.H. Lin, H.J. Hsu, R. Bartenschlager, W.B. Fischer, Membrane undulation induced by NS4A of dengue virus: a molecular dynamics simulation study, J. Biomol. Struct. Dyn. 32 (2013) 1552–1562.